Confinement-induced structural changes of water studied by Raman scattering

M. Erko,[1] G. H. Findenegg,[2] N. Cade,[3] A. G. Michette,[3] and O. Paris[1,*]

[1]*Institute of Physics, Montanuniversitaet Leoben, A-8700 Leoben, Austria*
[2]*Institute of Chemistry, TU Berlin, D-10623 Berlin, Germany*
[3]*Department of Physics, King's College London, WC2R 2LS London, United Kingdom*

The temperature dependence of water confined in the ordered cylindrical nanopores of MCM-41 and SBA-15 materials is studied by means of Raman scattering for different pore sizes covering a diameter range from 2.0 to 8.9 nm. The liquid–solid phase transition temperature of water in confinement can be determined by the analysis of the mode contribution in the OH-stretching region. For pore sizes down to 3 nm, the freezing/melting point depression with decreasing pore size can be consistently described by a modified Gibbs-Thomson equation, with a nonfreezable water layer of 0.6 nm (about two monolayers) close to the pore walls. When the pore size is 2.5 nm or smaller, indication for a first-order phase transition can no longer be found that is in agreement with previously reported differential scanning calorimetry measurements on the same samples. The Raman data further suggest that two spatially separated water phases exist in the smallest pores, i.e., the nonfreezable wall layer and a structurally different water phase in the core of the pores. A distinct tetrahedral hydrogen-bonded network of water molecules is found only in the core part of the pores. In the weakest confinement (8.9-nm pore diameter), the core water is shown to be compatible with crystalline ice with a spectral fingerprint similar to bulk ice. In strong confinement (2.0-nm pore diameter), the core water shows a spectral fingerprint identical to low-density amorphous ice, and there is a gradual transition between these two extremes. These findings suggest that the core part of confined water undergoes considerable structural changes with decreasing pore size, leading us to question recent proposals that aim to extract information about the state of bulk liquid water in the "no man's land" from water in confinement.

I. INTRODUCTION

The structure and dynamics of supercooled liquid water and of amorphous ice is an active area of current research.[1–4] Interest in this subject was amplified by recent evidence from computer simulations[5] for the existence of a liquid–liquid phase boundary between low- and high-density liquid phases. Unfortunately, direct experimental studies of this phenomenon are prevented by the inability to supercool bulk water <235 K due to homogeneous nucleation of crystalline ice[6]; thus, the relevant temperature range is not accessible ("no man's land").[2] When confining water within nanoscale pores, the liquid–solid phase transition can be shifted to a temperature well below the limit of homogeneous nucleation, and liquid water may be observed down to temperatures as low as 150 K. Using differential scanning calorimetry (DSC), it has recently been demonstrated that, for water confined in the cylindrical mesopores of MCM-41[7] and SBA-15[8] silica, the melting point decreases with decreasing pore diameter following a modified Gibbs-Thomson equation.[9–11] No DSC peaks were found for water confined in pores with diameters <3 nm,[9] indicating the suppression of the first-order liquid–solid phase transition under very strong confinement. Recent studies of water confined in nanopores <2 nm proposed using this "trick" to experimentally verify[12–14] the hypothesis about the existence of a liquid–liquid phase boundary ending in a second critical point of bulk water.[15,16] However, the behavior of water in nanoscale confinement differs significantly from that of bulk water. The presence of a surface changes its thermodynamic parameters by strongly modifying the water hydrogen-bonded (HB) network.[17,18] Therefore, experimental data from strongly confined water may not be suitable for predictions about the phase behavior of bulk water and require further experimental verification.

Numerous studies of water phase transitions in confinement have been performed with x-ray and neutron scattering.[19–24] Several studies indicated the formation of cubic ice in the silica mesopores instead of the hexagonal ice formed in the bulk.[25,26] However, diffraction studies give only indirect information about the existence of crystalline or amorphous states of water, because Bragg peaks of ice strongly broaden due to finite crystallite size, making it eventually impossible to distinguish unambiguously between the liquid and the solid states. Small-angle scattering of x-rays[27] and neutrons[13,28,29] have also been utilized, and the intensity changes of Bragg reflections from the ordered pore lattice of MCM-41 have been attributed to the density distribution of water within the pores. Information about the dynamics of supercooled water can be obtained from inelastic and quasielastic neutron scattering[30,31] or nuclear magnetic resonance (NMR).[32–34] In addition, Fourier-transform infrared (FTIR) and Raman spectroscopy can provide information on the vibrational dynamics of water molecules. In particular, the broad OH-stretching (OHS) region of water originating from different partially overlapping vibration modes has been analyzed in detail and refined over the years for different temperature regions.[35–39] At room temperature, the OHS spectrum of bulk liquid water is described by four peaks: (I) 3250 cm^{-1}, (II) 3420 cm^{-1}, (III) 3545 cm^{-1}, and (IV) 3635 cm^{-1}. The four OHS modes reflect the different intermolecular bonding degrees, ranging from fully HB ones in mode I to the almost free molecules in mode IV.[38] Modes III and IV are most pronounced at high temperatures and decline at lower temperatures.[40] For temperatures <280 K, a new component, mode V, arises at

$\sim$3100 cm^{-1}, representing the OHS contribution of water molecules forming the icelike tetrahedral HB network. The occurrence of this "ice-peak" has been attributed to the existence of crystalline ice as heterophase fluctuation in supercooled bulk water.[39]

In this work, we present a systematic experimental investigation of the effect of confinement on the phase behavior of water between 123 and 293 K using Raman scattering. We use the same ordered mesoporous hydrophilic silica samples as in Ref. [9], which cover pore diameters from 2.5 to 8.9 nm, and an additional MCM-41 sample with a pore diameter of 2.0 nm. We determine and analyze the position, width, and relative peak area of the HB mode V in the OHS part of the Raman spectrum as a function of temperature and pore diameter. Furthermore, we use the spectral position of the mode I OHS contribution to estimate the phase transition temperature for pore diameters >2.5 nm. The results are compared with literature values for bulk (hexagonal) crystalline ice and for bulk amorphous ice and are discussed with respect to the influence of confinement on the low-temperature phase behavior of water.

II. EXPERIMENT

Ordered mesoporous silica materials MCM-41[7] and SBA-15[8] were used as confining matrices in the present work. These materials exhibit a two-dimensional hexagonal arrangement of cylindrical pores of uniform size with diameters of $\sim$2–5 nm (MCM-41) and 5–10 nm (SBA-15). The synthesis of these materials is based on the self-assembly of surfactants (MCM-41) or block copolymers (SBA-15) in the presence of a silica precursor (tetraethoxysilane) and is described in detail elsewhere.[9,11,41] The resulting materials were chemically pure, amorphous silica, as ensured by the high calcination temperature of 550 °C to remove the organic template,[9,11] with different amounts of hydroxyl groups decorating the pore surface.[42] NMR has shown that for similar samples synthesized within the same group, all hydrogen atoms are either surface SiOH groups or HB water molecules.[32] We used five MCM-41 samples, denoted as MCM20, MCM25, MCM30, MCM34, and MCM44, and one SBA-15 sample, denoted as SBA89, where the numbers indicate the pore diameter (in angstroms) determined by the Kruk-Jaroniec-Sayari (KJS) method.[9]

The pore space of the silica powder samples was filled with deionized water at ambient pressure by imbibition of the liquid. The specific amount of water required to completely fill the pore space is known from earlier adsorption experiments.[9,28] The filling fraction was chosen to be slightly less than unity to avoid bulk water outside the pores. Temperature control of the samples was realized by a liquid nitrogen–based Linkam THMS 600 cooling stage operating between 110 and 310 K. Each sample was enclosed in a glass sample cell inside the cooling stage, surrounded by a nitrogen atmosphere. One cooling cycle and one heating cycle were performed for each sample in the temperature range between room temperature and 123 K. The cooling/heating rate was 1 K/min. Raman spectra were recorded at a constant temperature in steps of 10 K after temperature equilibration. As a reference, a measurement with a single water droplet representing the bulk water state

was performed under exactly the same experimental conditions as those used for water confined in the nanopores.

Raman backscattering measurements were performed at ambient pressure in the spectral region between 100 and 4200 cm^{-1} using a micro-Raman spectrometer (Renishaw 1000). Samples were illuminated with a 514-nm laser (Innova 70C) at 300 mW, using a 40$\times$ objective (Nikon, ELWD 0.6 NA). Spectra were recorded with a charge-coupled device camera at a resolution of 1 cm^{-1}, with a total exposure time of 215 s for each spectrum. Peak analysis was performed with the Renishaw Wire 3.1 fitting software, after baseline subtraction.

III. RESULTS

A. Raman spectra

The measured Raman spectra are dominated by a broad and intensive signal in the range 3000–3700 cm^{-1}, which can be attributed to the water OHS mode.[43] Room temperature spectra of the OHS region for bulk water (water droplet) and water confined in MCM25 (2.5-nm pore diameter) are shown in Fig. [1]. Also shown is the room temperature spectrum of dry MCM25 which was recorded in a stream of dry nitrogen gas. The OHS spectrum shows significant changes with temperature (Fig. [2]) and as a function of confinement in the pores (see Fig. [4]). In addition to the water OHS signal, two sharp peaks appear between 2900 and 3000 cm^{-1}. This double peak is also present for the empty MCM25 sample but is absent for the water droplet and should therefore be attributable to the mesoporous matrix. Similar spectral features were already reported and discussed in the literature, but their physical origin still seems to be a matter of debate. Because the spectral position is roughly consistent with CH stretching, it has been attributed to hydrocarbon impurities remaining from the surfactant after calcination.[44] However, because our samples were calcined at 550 °C, we do not expect any hydrocarbon impurities. A different description implies
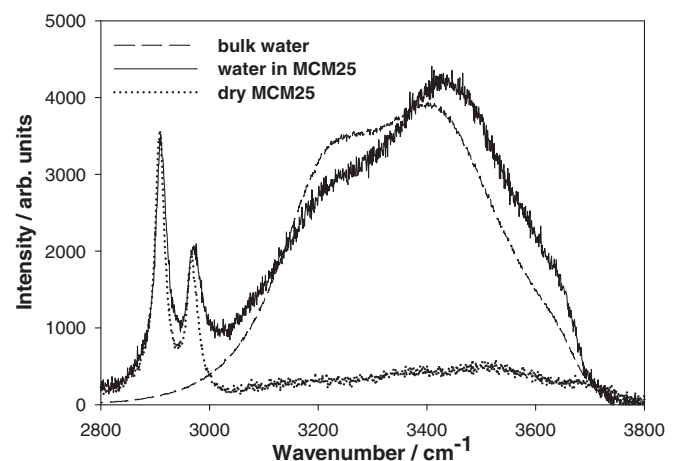
FIG. 1. Experimental Raman OHS spectra measured at room temperature. The bulk water spectrum, represented by the measurement of the water droplet, is shown by the dashed line. The solid line is the spectrum measured for water confined in MCM25 (2.5-nm-wide pores). The two sharp peaks at low wave numbers arise from the mesoporous matrix, as indicated by an independent measurement of dry MCM25 (dotted line).
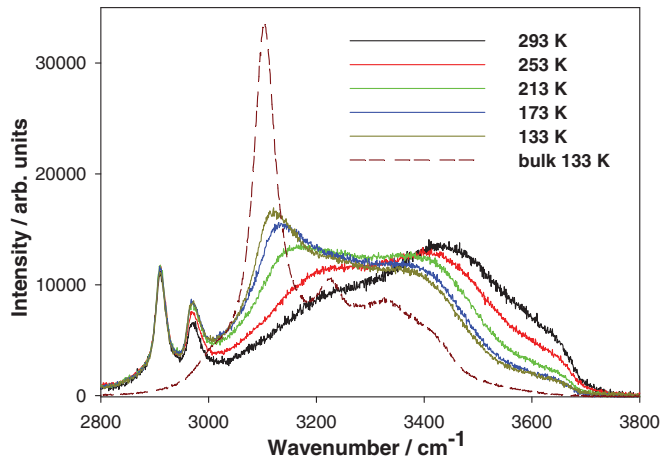
FIG. 2. (Color online) Experimental Raman OHS spectra measured for water in MCM25 (2.5-nm-wide pores) for different temperatures (solid lines), together with the experimental bulk ice spectrum at 133 K (dashed line).

laser radiation–induced defects (silanone, i.e., $Si = O$ double bonds),[45] which seems to be a more plausible explanation. In our case, the two sharp peaks showed some minor variation for the different samples, but no temperature dependence was observed. This leads us to the conclusion that these peaks are not associated with the OHS spectrum of water. Hence, we do not discuss them further in the subsequent analysis. From Fig. 2, we see that the tail of the water OHS spectrum slightly enters the region of these two peaks. Therefore, the two peaks were fitted together with the water spectrum (described later). A cross-check for some datasets revealed that the analysis is robust irrespective of whether the peaks are taken into account in peak fitting or not.

Deconvolution of the broad OHS Raman spectrum was performed using four or five Gaussian functions, depending on the temperature. As an example, a fit of the spectrum of water confined in MCM25 at 143 K is shown in Fig. 3. They are attributed to the OHS modes I–IV, with their spectral position ranging from ~ 3200 cm^{-1} (mode I) to ~ 3650 cm^{-1} (mode IV), in accordance with reports in the literature.[14,38,46,47] At low temperatures, an additional component (mode V)
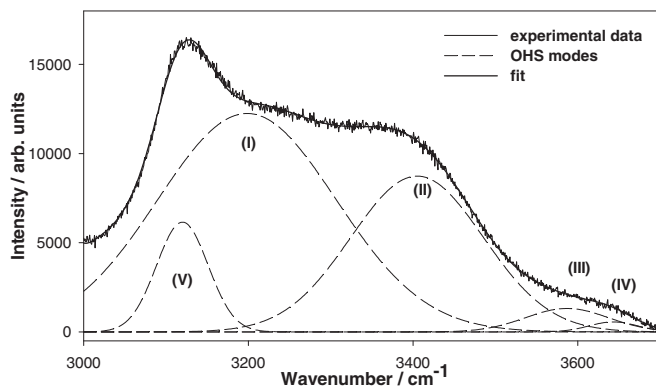
FIG. 3. Deconvolution of the OHS region for water confined in MCM25 at 143 K: experimental data (thin solid line), fit function (thick solid line), and the five components (modes I–V) (dashed lines).
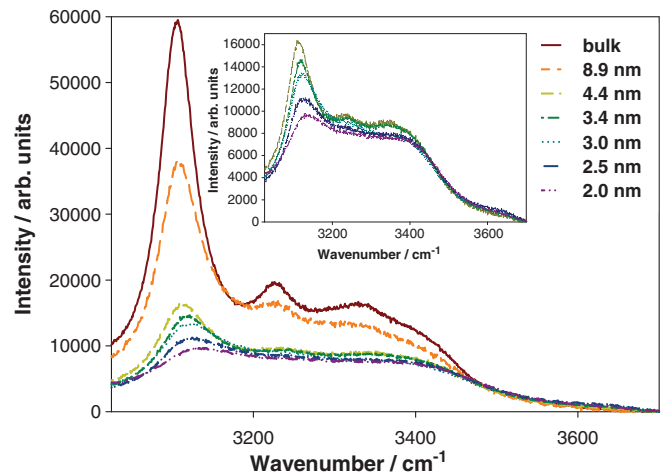
FIG. 4. (Color online) Raman OHS spectra of water in different confinement at 143 K. The spectral contribution of mode V that occurs ~ 3100 nm^{-1} decreases monotonically with decreasing pore size. The inset shows magnified spectra of samples with pore sizes between 2.0 and 4.4 nm.

appears somewhat below mode I (3100 cm^{-1}). This peak is attributed to the formation of a tetrahedral HB network, as in hexagonal, cubic, and (low density) amorphous ice, and is referred to as ice-peak.[36,37,46,48,49] For all samples, the spectral characteristics (peak position, peak width, and intensity) of all OHS components change with temperature. Figure 2 demonstrates that lowering the temperature causes a spectral shift to lower wave numbers (redshift) and a sharpening of the mode V component is observed. Furthermore, the intensities of modes I and V were found to increase relative to those of modes II–IV as the temperature decreases.

For water confined in the pores, the peak characteristics of the OHS spectrum are changing with the degree of confinement. In SBA89, the material with the widest pores (8.9-nm diameter) in the OHS spectrum largely resembles the features of the one for the water droplet (bulk water) at the same temperatures. As the pore size decreases, a blueshift of the mode V contribution and a broadening of the entire OHS water spectrum are observed, as demonstrated in Fig. 4 for a given temperature of 143 K.

The spectral characteristics (peak position, peak width, and intensity) of all components of the OHS spectrum of bulk water (water droplet) and water confined in pores of the six silica materials were determined from the spectral fits for the entire experimental temperature range. Major changes are observed for the low-wave-number contributions, or modes I and V. Modes II–IV did not exhibit such significant systematic changes with temperature or pore size. Therefore, a detailed analysis was performed only for OHS modes I and V.

B. Freezing and melting in confinement

The OHS spectrum of bulk water (water droplet) exhibits significant changes upon freezing and melting. The position, as well as the peak width, of mode I changes in a discontinuous way at the phase transition temperature during the cooling and
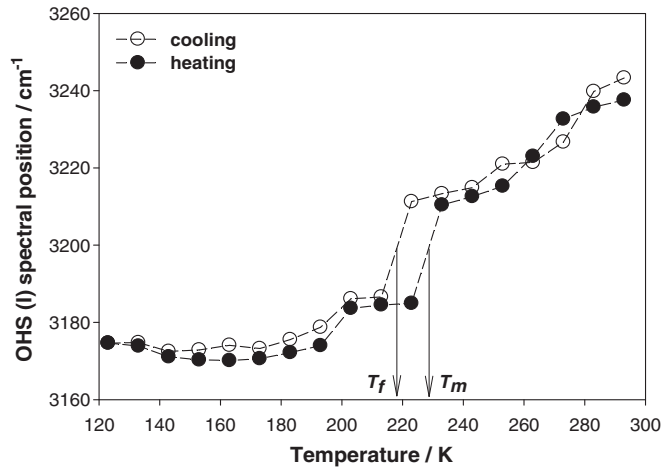
FIG. 5. Fitted spectral position for OHS mode I of water confined in 3.4-nm pores. Open and filled circles indicate the cooling and heating directions, respectively. The freezing and melting temperatures, T_f and T_m, respectively, are assigned to the midpoints of the interval before and after the discontinuous change.

FIG. 6. Correlation of the melting temperature T_m with an effective pore radius $R - t$, assuming a layer thickness $t = 0.6$ nm of nonfreezable water. Crosses mark the DSC data from Refs. 9 and 11; points are obtained by the present Raman data analysis. The dashed line illustrates the linear regression described by Eq. (2).

melting cycles. For confined water, a similar stepwise change of the mode I component is found as long as the pore diameter is not too small. Figure 5 shows exemplary the results for MCM34. The discontinuous step in the peak position is clearly observed occurring ~220 K upon cooling and occurring ~230 K upon heating. As the pore size decreases, the step occurs at a lower temperature and the step height decreases. For water confined in the sample of the 2.5-nm pore diameter, this step is at the limit of experimental detectability, and for the sample of the 2.0-nm pore size, all fitted parameters of the OHS mode I change smoothly with temperature.

The OHS spectrum of bulk ice is dominated by the intensity of mode V[36,48] (see Figs. 2 and 4), which is absent in the liquid range at high temperatures. For the bulk water droplet, it appears at 263–253 K upon cooling, and it vanishes at 263–273 K upon heating, in perfect agreement with the step in mode I. The temperature at which the mode V peak first appears in confinement decreases with decreasing pore size. Therefore, not only the discontinuous change in the position and width of mode I but also the appearance of mode V seem to be indicative for the liquid–solid phase transition of water. However, at low-enough temperatures, the mode V peak is present in all samples—including the one with smallest pores (2.0 nm), for which no step was found by the analysis of mode I. Experimental evidence for mode V in supercooled liquid bulk water was also reported in Ref. 39. Therefore, we conclude that the first appearance of mode V should not be taken as unique indication of the liquid–solid phase transition of confined water. Instead, we take the discontinuous change in the position of mode I to estimate the phase transition temperature. According to current models,[38,46,48] mode I represents the symmetric stretching vibration of strongly HB water molecules that are already present in the liquid state. The Raman intensity of this mode is strong in both the liquid and the solid states; therefore, data analysis of the whole measured temperature range between room temperature and 123 K could be performed with high accuracy.

The confinement-induced shift of the melting temperature, $\Delta T_m = T_0 - T_m$, for water in a series of MCM-41 and SBA-15 materials was recently studied by Findenegg *et al.* using DSC.[10] They found that ΔT_m can be related to the pore radius R by a modified form of the thermodynamic Gibbs-Thomson equation

$$\Delta T_m = \frac{C}{R - t}, \quad \text{with} \quad C = C_{GT} = \frac{2T_0\gamma_{sl}v_l}{\Delta h_{sl}}, \quad (1)$$

where the parameter t was introduced to account for a layer of nonfreezable water at the pore walls. A good representation of the DSC data was obtained with $t = 0.6$ nm, which corresponds to about two monolayers of nonfreezing water molecules adjacent to the pore walls.[9,10] From our Raman scattering results, we define the phase transition temperature in the pores by the discontinuous change of the spectral position of the OHS mode I (Fig. 5). The nominal freezing and melting temperatures of water in a given sample were defined operationally as the midpoint of the interval before and after the discontinuous change of the OHS mode I spectral position. Because the spectra were taken in 10-K steps, the transition temperatures have error bars of ± 5 K. To check whether the phase transition temperature T_m derived from the temperature dependence of the Raman OHS mode I conform to this simple relation, Eq. (1) was applied in the form

$$T_m(R - t) = T_0(R - t) - C_{GT}. \quad (2)$$

A plot of the resulting melting temperatures according to Eq. (2), with $t = 0.6$ nm, is shown in Fig. 6, together with the respective results from the DSC measurements taken from the literature.[9,11] The graph shows that the results from Raman scattering are in excellent agreement with those of the DSC study. The value of the Gibbs-Thomson constant derived from the analysis of the OHS mode I on the basis of Eq. (2), $C = 63 \pm 8$ K nm, agrees within the limits of error with the respective value from the DSC study, $C = 53 \pm 1$ K nm. As in the DSC study, no clear discontinuity indicating a first-order
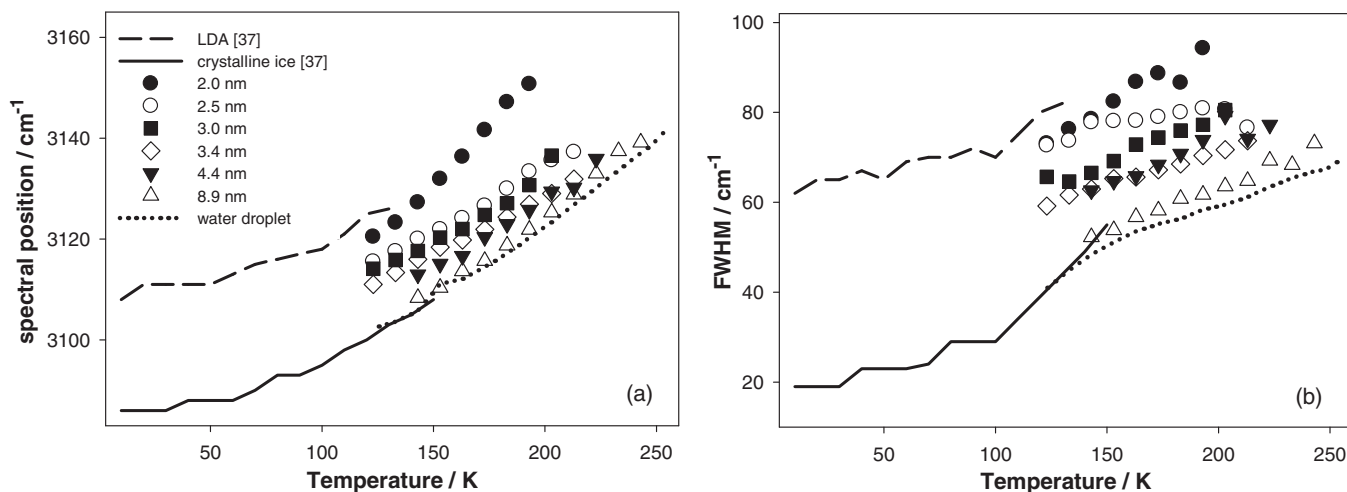
FIG. 7. Temperature dependence of the ice-peak characteristics for confinement in pores of different sizes. (a) Fitted spectral position, and (b) FWHM for the measurements of the single water droplet (dotted line) and for water in six confinement dimensions (symbols). Also shown are the data attributed to crystalline (solid line) and amorphous (dashed line) solid water from Ref. 37.

phase transition could be obtained for samples with diameter of 2.5 nm and below.

C. Analysis of the ice-peak

Another remarkable finding becomes apparent from the detailed analysis of the mode V contribution as a function of temperature and confinement. As mentioned earlier, this mode represents strongly HB oscillators in an icelike tetrahedral water network, as present in hexagonal, cubic, and (low density) amorphous ice. We therefore denote this peak as ice-peak in the following. Figure 7 shows the spectral position and width (full width at half maximum, or FWHM) of the ice-peak plotted as a function of temperature for samples of different pore widths. For all samples, the peak position shifts to a lower wave number and the peak width decreases as the temperature decreases. Figure 7 also shows that decreasing the pore size at a given temperature causes a shift of the peak position to higher wave numbers [Fig. 7(a)] and a broadening of the peak [Fig. 7(b)]. Raman and FTIR OHS spectra of bulk crystalline ice and low-density amorphous ice (LDA) have been reported in earlier studies.[36,37] The values of the spectral position and width of the ice-peak of crystalline and amorphous bulk ice reported in Ref. 37 are included in Figs. 7(a) and 7(b). Apparently, these two curves seem to determine the bounds of our experimental data, with water in the 8.9-nm pores almost corresponding to bulk crystalline ice and water in the 2.0-nm pores almost corresponding to vapour-deposited LDA.

Further analysis of the OHS spectrum also reveals that the intensity contribution of the ice-peak, defined as the ratio of the area of mode V divided by the total OHS area, changes with the degree of confinement of water (see also Fig. 4). At a given temperature, the relative contribution of the ice-peak is largest for water in the widest pores and decreases systematically with decreasing pore size. This relation holds for the entire temperature range in which the ice-peak is observed. The relative peak area can be taken as a measure for the fraction of

molecules in the respective vibrational mode. Hence, we may infer that there are two populations of water molecules in the pores: one forming a strong HB tetrahedral water network and the other not forming such network. On the basis of the results presented in Fig. 6, we propose that these two populations represent the water in the core of the pores and the layer of nonfreezable water at the pore walls, which is often termed interfacial water.[4] Assuming that the layer thickness t is independent of the pore radius R, as suggested by Fig. 6, and that a layer of similar thickness exists in the smallest pores, we can estimate the volume fraction of water in the core of the pores, which we call core water, by $\varphi_b = (R - t)^2/R^2$. A plot of the relative area of the ice-peak versus the volume fraction of core water, adopting a layer thickness $t = 0.6$ nm, is shown in Fig. 8 for a fixed temperature of 173 K. Remarkably, a linear relationship is obtained for the entire
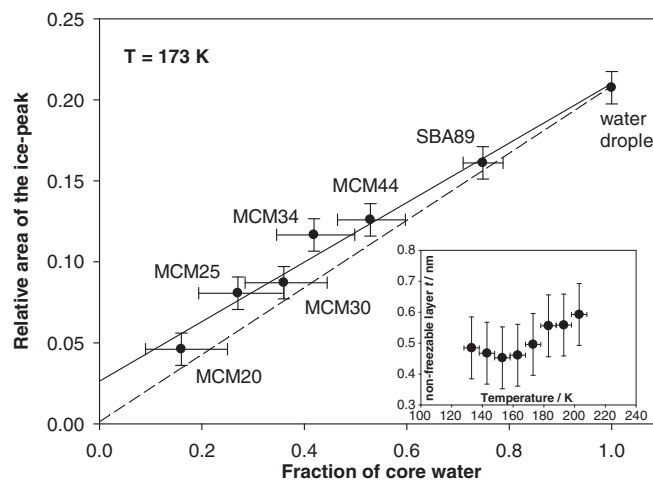
FIG. 8. The relative area of the ice-peak is directly proportional to the fraction of core water within the pores of different sizes. The solid line is a linear fit for $t = 0.6$ nm. The dashed line shows the fit for a decrease of the layer thickness t by 0.1 nm. The inset shows the temperature dependence of t.

set of samples, including those with smallest pore diameters (2.5 and 2.0 nm) and the bulk water droplet, for which the fraction of core water was set to 1. A linear relationship as in Fig. 8 holds for all temperatures for the set of samples in which the ice-peak was present at that particular temperature. The error bars in Fig. 8 indicate the estimated error in the determination of the relative area of the ice-peak (vertical bars) and the changes in the calculated fraction of core water resulting from an estimated uncertainty of the layer thickness t of nonfreezable water of 0.1 nm (horizontal bars). The linear relation between the relative peak area of the ice-peak and the volume fraction of the core water also holds for these higher or lower values of the layer thickness. Moreover, the graph for the lower layer thickness ($t = 0.5$ nm), indicated by the dashed line in Fig. 8, passes through the origin—as would be expected if the nonfreezable wall layer is assumed not to contribute to the ice-peak. The appropriate values for the nonfreezable layer thickness for other temperatures are shown in the inset of Fig. 8. The deviation of our Raman OHS data from the DSC data in Fig. 6 in this case is still well within the combined experimental uncertainty of the two independent methods.

IV. DISCUSSION

We performed a systematic study of the effect of confinement on freezing and melting of water in cylindrical silica nanopores using Raman scattering. These findings confirm results from earlier studies[37,39,43,50–52] and allow us to draw new conclusions based on the systematic change of confinement dimensions from 8.9 to 2 nm.

Raman spectra in the OHS region of water show pronounced changes in the population of the individual stretching modes on confinement. At room temperature, the population of high-energy vibrations increases with confinement (Fig. 1). This high-energy contribution can be attributed to weakly connected water molecules.[38,46] Accordingly, confinement appears to weaken the connectivity of the HB network of water molecules, resulting in an increase of their mobility. This effect is consistent with results from NMR measurements.[53,54] Significant changes of the OHS Raman signal are observed during cooling and heating in the temperature range between 123 and 303 K. The temperature-induced changes in the OHS spectrum are indicative for the changes of the intramolecular bonding within the water network. The position and width, as well as the relative intensities of all spectral components, change systematically with temperature. With decreasing temperature, the non-HB oscillations are successively replaced by those of a HB network, leading to a relative increase of the intensity of the components with lower wave numbers. This temperature-induced change in the network of water molecules also influences the strength of the molecular oscillators and leads to a shift in the spectral position of the OHS modes. Temperature-induced ordering and disordering of water molecules lead to, respectively, narrowing and broadening of each contribution peak. These effects also show a systematic dependence on confinement dimensions.

For bulk water and water confined in pores >2.5 nm, the development of the OHS mode I contribution with temperature can be used to determine the liquid–solid phase transition

temperature from the discontinuous change of the spectral position (Fig. 5) and the width of the peak (data not shown). Phase transition temperatures obtained by this method are in excellent agreement with those from DSC measurements performed independently on the same samples.[9,10] This close agreement confirms the finding in Ref. 9 that the parameter C of Eq. (1) agrees reasonably with the Gibbs-Thomson constant as derived from thermodynamic parameters of bulk water: $C_{GT} = 2T_0 \gamma_{sl} \nu_l / \Delta h_{sl} = 54$ K nm, where T_0 is the melting temperature, γ_{sl}, is the free energy per unit area of the liquid–solid interface, ν_l is the molar volume of the liquid phase, and Δh_{sl} is the molar enthalpy of melting. It is remarkable that the thermodynamic Gibbs-Thomson equation is applicable down to the nanometer regime when we allow for the existence of a nonfreezable layer of water at the pore walls. In agreement with the DSC study, we find that at the pore walls of hydrophilic silica in MCM-41 and SBA-15, the thickness of this layer corresponds to about two monolayers of water molecules. Strong interfacial-bound water layers of similar thickness where also reported for Vycor porous glass,[55] and the existence of a quasiliquid water layer was reported for planar silica surfaces.[56]

The magnitude of the discontinuous step in the spectral position and width of the OHS mode I decreases with decreasing pore size, showing essentially the same trend as the exothermic/endothermic heat transfer measured in DSC.[9] For water confined in pores of a 2.5-nm diameter, a slight discontinuity in the spectrum is perhaps present but is no longer quantifiable. In pores of a 2.0-nm diameter, both the position and the width of the OHS mode I change smoothly with temperature in the range between 123 and 303 K. This observation supports the conjecture of a continuous liquid–solid phase transition of water in narrow pores.[24] This effect should in some way be connected to the existence of a nonfreezing water layer close to the pore wall. To assess the significance of the vanishing step in the OHS mode I parameters more quantitatively, the step height should be normalized by the amount of water in the core volume. A nonfreezing water layer of a 0.6-nm thickness in pores of a 2.5- or 2.0-nm diameter leaves a core volume fraction of 27% and of 16%, respectively, in which the water may freeze. In both cases, the amount of water in the core volume is well above the limit of experimental resolution of DSC and Raman measurements. The analysis of the DSC data revealed that the (molar) enthalpy of melting Δh_{sl} of water sharply decreases with decreasing core radius ($R - t$) and disappears at an estimated pore diameter of 2.7 nm.[9] The value of the limiting pore diameter derived from the DSC data in this way somewhat depends on the value of the layer thickness t, which can only be determined indirectly. In this respect, the determination of the limiting pore diameter from the Raman OHS spectra is more direct, because it is based on the direct detection of the disappearance of a step in the position and width of the mode I spectra. In this way we definitively found that no first-order phase transition occurs in pores of diameters <2.5 nm. Hence, the two methods yield concordant results for the limiting pore diameter of a first-order freezing transition of water.

In this context, the population of the ice-peak (mode V) scales linearly with the estimated fraction of core water, according to $\varphi_b = (R - t)^2 / R^2$, when assuming the same

value of the layer thickness of nonfreezing water as in the analysis of the mode I spectra (Fig. 8). Although a slight temperature dependence of t seems to be present (inset in Fig. 8), this result suggests that water in the pores consists of two spatially separated phases irrespective of the pore size. The interfacial water near the pore walls consists of non-or weakly HB water molecules, contributing essentially to the high-energy part of the OHS spectrum (modes II–IV). The relative fraction of water in the core of the pore space consequently decreases with decreasing pore size. From the viewpoint of dynamics, this seems to imply that there should be no essential difference in the dynamic behavior of bulk water and confined core water, even in very small pores. In a similar context, the term "free" water with bulklike properties was introduced by Gallo *et al.*[57,58] and was used to argue that results obtained from strongly confined water can be taken to predict bulk water behavior in the no man's land.[59] However, an important conclusion from the analysis of the Raman ice-peak is that the structure of water in the core of the pores changes with the degree of confinement, which should therefore not be considered bulklike. This follows from a comparison of the parameters of the ice-peak in the pores with the corresponding values for bulk samples of crystalline ice and vapour-deposited LDA reported by Sivakumar *et al.*[37] This in turn leads to the conclusion that, upon cooling, the core water in large pores undergoes a first-order phase transition, forming crystalline ice similar to bulk ice. For water confined in pores of a smaller pore size, a shift of the spectral position and peak width toward the values attributed to LDA as reported in Refs. 36 and 37 is observed. In the pores of a 2.0-nm diameter, we observe a signal that corresponds closely to the one of bulk LDA. From this, we conclude that there is a continuous transition from crystalline ice for weak confinement (8.9-nm pores) to LDA for strong confinement (2-nm pores). Hence, our results indicate a confinement-induced structural change of the core water with decreasing pore size. A similar continuous transition of confined water from liquid to solid has previously been reported from x-ray diffraction measurements and was interpreted as a "new type of phase transition."[24]

Finally, distinct differences in the dynamics of bulk water and confined water can also be deduced from the spectral region around 1600 cm^{-1}, which represents the HOH-bending mode of water molecules. For bulk water, the disappearance of the HOH-bending peak upon freezing has been attributed to the sudden increase of the molecular connectivity.[60] In our experiments (data not shown), the HOH-bending peak was present at all temperatures down to 123 K, even in the widest pores of the SBA-15 sample (8.9-nm pore diameter). Only for the bulk water droplet did the HOH peak completely vanish upon freezing, in accordance with other investigations. Therefore, we stress that this spectral signature (similar to the appearance/disappearance of the ice-peak) cannot be used to uniquely determine the liquid state of water in pores, as was proposed in Ref. 14. Nevertheless, further work is needed for a more quantitative analysis of the effect of confinement on the weak HOH-bending signal.

V. CONCLUSIONS

We presented experimental evidence that the strong interaction of water molecules with the walls of the cylindrical nanopores of SBA-15 and MCM-41 leads to a nonfreezable water layer of ~0.6-nm thickness. This layer contributes to the high-energy part of the OHS spectrum only, indicating a weakly HB water structure without any tetrahedral coordination. In contrast, the water confined within the core of the cylindrical pores shows at low temperatures the fingerprint of HB, tetrahedrally coordinated water represented by the Raman mode V or ice-peak in the low-energy region of the OHS spectrum. This core water shows a continuous structural change from crystalline ice for large (8.9 nm) pores toward LDA for very small (2 nm) pores. In view of these two spatially separated water populations in the pores, and because the intrinsic structure of the core water depends on the degree of confinement, we conclude that it will be rather difficult to extract information about the state of bulk liquid water in the no man's land from studies of water confined in nanopores.[1]

---

*oskar.paris@unileoben.ac.at

[1]O. Mishima and H. E. Stanley, Nature **396**, 329 (1998).

[2]P. G. Debenedetti and H. E. Stanley, Phys. Today **56**, 40 (2003).

[3]A. K. Soper, Mol. Phys. **106**, 2053 (2008).

[4]I. Brovchenko and A. Oleinikova, *Interfacial and Confined Water* (Elsevier, Amsterdam, 2008).

[5]L. M. Xu, P. Kumar, S. V. Buldyrev, S. H. Chen, P. H. Poole, F. Sciortino, and H. E. Stanley, Proc. Natl. Acad. Sci. USA **102**, 16558 (2005).

[6]R. J. Speedy and C. A. Angell, J. Chem. Phys. **65**, 851 (1976).

[7]C. T. Kresge, M. E. Leonowicz, W. J. Roth, J. C. Vartuli, and J. S. Beck, Nature **359**, 710 (1992).

[8]D. Y. Zhao, J. L. Feng, Q. S. Huo, N. Melosh, G. H. Fredrickson, B. F. Chmelka, and G. D. Stucky, Science **279**, 548 (1998).

[9]S. Jahnert, F. V. Chavez, G. E. Schaumann, A. Schreiber, M. Schonhoff, and G. H. Findenegg, Phys. Chem. Chem. Phys. **10**, 6039 (2008).

[10]G. H. Findenegg, S. Jahnert, D. Akcakayiran, and A. Schreiber, ChemPhysChem **9**, 2651 (2008).

[11]A. Schreiber, I. Ketelsen, and G. H. Findenegg, Phys. Chem. Chem. Phys. **3**, 1185 (2001).

[12] S. H. Chen, L. Liu, E. Fratini, P. Baglioni, A. Faraone, and E. Mamontov, Proc. Natl. Acad. Sci. USA **103**, 9012 (2006).

[13] D. Z. Liu, Y. Zhang, C. C. Chen, C. Y. Mou, P. H. Poole, and S. H. Chen, Proc. Natl. Acad. Sci. USA **104**, 9570 (2007).

[14] F. Mallamace, M. Broccio, C. Corsaro, A. Faraone, D. Majolino, V. Venuti, L. Liu, C. Y. Mou, and S. H. Chen, Proc. Natl. Acad. Sci. USA **104**, 424 (2007).

[15] H. E. Stanley, P. Kumar, S. Han, M. G. Mazza, K. Stokely, S. V. Buldyrev, G. Franzese, F. Mallamace, and L. Xu, J. Phys. Condens. Matter **21**, 504105 (2009).

[16] H. E. Stanley, S. V. Buldyrev, P. Kumar, F. Mallamace, M. G. Mazza, K. Stokely, L. Xu, and G. Franzese J. Non-Cryst. Solids **357**, 629 (2011).

[17] W. Drost-Hansen, Chem. Phys. Lett. **2**, 647 (1968).

[18] K. Yoshida, T. Yamaguchi, S. Kittaka, M. C. Bellissent-Funel, and P. Fouquet, J. Chem. Phys. **129** (2008).

[19] M. C. Bellissent-Funel, J. Phys. Condens. Matter **13**, 9165 (2001).

[20] J. Seyed-Yazdi, H. Farman, J. C. Dore, J. B. W. Webber, G. H. Findenegg, and T. Hansen, J. Phys. Condens. Matter **20**, 205108 (2008).

[21] B. Webber and J. Dore, J. Phys. Condens. Matter **16**, S5449 (2004).

[22] C. Alba-Simionesco, B. Coasne, G. Dosseh, G. Dudziak, K. E. Gubbins, R. Radhakrishnan, and M. Sliwinska-Bartkowiak, J. Phys. Condens. Matter **18**, R15 (2006).

[23] J. Deschamps, F. Audonnet, N. Brodie-Linder, M. Schoeffel, and C. Alba-Simionesco, Phys. Chem. Chem. Phys. **12**, 1440 (2010).

[24] K. Morishige and K. Kawano, J. Chem. Phys. **110**, 4867 (1999).

[25] M. C. Bellissentfunel, J. Lal, and L. Bosio, J. Chem. Phys. **98**, 4246 (1993).

[26] K. Morishige and K. Nobuoka, J. Chem. Phys. **107**, 6965 (1997).

[27] J. Prass, D. Muter, P. Fratzl, and O. Paris, Appl. Phys. Lett. **95** (2009).

[28] M. Erko, D. Wallacher, A. Brandt, and O. Paris, J. Appl. Crystallogr. **43**, 1 (2010).

[29] R. Mancinelli, S. Imberti, A. K. Soper, K. H. Liu, C. Y. Mou, F. Bruni, and M. A. Ricci, J. Phys. Chem. B **113**, 16169 (2009).

[30] M. C. Bellissent-Funel, Eur. Phys. J. E **12**, 83 (2003).

[31] S. H. Chen, F. Mallamace, C. Y. Mou, M. Broccio, C. Corsaro, A. Faraone, and L. Liu, Proc. Natl. Acad. Sci. USA **103**, 12974 (2006).

[32] B. Grunberg, T. Emmler, E. Gedat, J. Shenderovich, G. H. Findenegg, H. H. Limbach, and G. Buntkowsky, Chem. Eur. J. **10**, 5689 (2004).

[33] F. Mallamace, C. Corsaro, M. Broccio, C. Branca, N. Gonzalez-Segredo, J. Spooren, S. H. Chen, and H. E. Stanley, Proc. Natl. Acad. Sci. USA **105**, 12725 (2008).

[34] E. W. Hansen, M. Stocker, and R. Schmidt, J. Phys. Chem. **100**, 2195 (1996).

[35] G. E. Walrafen, J. Chem. Phys. **47**, 114 (1967).

[36] C. G. Venkatesh, S. A. Rice, and J. B. Bates, J. Chem. Phys. **63**, 1065 (1975).

[37] T. C. Sivakumar, S. A. Rice, and M. G. Sceats, J. Chem. Phys. **69**, 3468 (1978).

[38] Q. Sun, Vib. Spectros. **51**, 213 (2009).

[39] G. D'Arrigo, G. Maisano, F. Mallamace, P. Migliardo, and F. Wanderlingh, J. Chem. Phys. **75**, 4264 (1981).

[40] C. I. Ratcliffe and D. E. Irish, J. Phys. Chem. **86**, 4897 (1982).

[41] G. A. Zickler, S. Jahnert, W. Wagermaier, S. S. Funari, G. H. Findenegg, and O. Paris, Phys. Rev. B **73**, 184109 (2006).

[42] I. G. Shenderovich, G. Buntkowsky, A. Schreiber, E. Gedat, S. Sharif, J. Albrecht, N. S. Golubev, G. H. Findenegg, and H. H. Limbach, J. Phys. Chem. B **107**, 11924 (2003).

[43] G. E. Walrafen, J. Chem. Phys. **40**, 3249 (1964).

[44] J. L. Blin and C. Carteret, J. Phys. Chem. C **111**, 14380 (2007).

[45] A. S. Zyubin, A. M. Mebel, S. H. Lin, and Y. D. Glinka, J. Chem. Phys. **116**, 9889 (2002).

[46] J. B. Brubach, A. Mermet, A. Filabozzi, A. Gerschel, and P. Roy, J. Chem. Phys. **122** (2005).

[47] G. E. Walrafen, M. R. Fisher, M. S. Hokmabadi, and W. H. Yang, J. Chem. Phys. **85**, 6970 (1986).

[48] J. E. Bertie and E. Whalley, J. Chem. Phys. **40**, 1637 (1964).

[49] S. A. Rice and M. G. Sceats, J. Phys. Chem. **85**, 1108 (1981).

[50] T. C. Sivakumar, D. Schuh, M. G. Sceats, and S. A. Rice, Chem. Phys. Lett. **48**, 212 (1977).

[51] K. Furic and V. Volovsek, J. Mol. Struct. **976**, 174 (2010).

[52] T. C. Sivakumar, H. A. M. Chew, and G. P. Johari, Nature **275**, 524 (1978).

[53] J. B. W. Webber, J. C. Dore, J. H. Strange, R. Anderson, and B. Tohidi, J. Phys. Condens. Matter **19**, 415117 (2007).

[54] E. Liu, J. C. Dore, J. B. W. Webber, D. Khushalani, S. Jahnert, G. H. Findenegg, and T. Hansen, J. Phys. Condens. Matter **18**, 10009 (2006).

[55] S. Gruener, T. Hofmann, D. Wallacher, A. V. Kityk, and P. Huber, Phys. Rev. E **79**, 067301 (2009).

[56] S. Engemann, H. Reichert, H. Dosch, J. Bilgram, V. Honkimaki, and A. Snigirev, Phys. Rev. Lett. **92**, 205701 (2004).

[57] P. Gallo, M. Rovere, and S. H. Chen, J. Phys. Chem. Lett. **1**, 729 (2010).

[58] P. Gallo, M. Rovere, and S. H. Chen, J. Phys. Condens. Matter **22**, 284102 (2010).

[59] L. M. Xu, F. Mallamace, Z. Y. Yan, F. W. Starr, S. V. Buldyrev, and H. E. Stanley, Nature Phys. **5**, 565 (2009).

[60] F. Franks, *Water: A Comprehensive Treatise* (Springer, New York, 1975), Vol. 5, p. 366.